Integrated analysis of gut microbiota structure and metabolic function in patients with cirrhosis and refractory ascites

DIANYAN CHEN[1], SANDU LIU[1], KA ZHANG[2], KE PAN[1], LINSU ZHANG[3], DEYUN SHU[1], JIN ZHANG[4] and DINGYAO REN[1]

[1]Department of Hepatology, The People's Hospital of Qiannan, Duyun, Guizhou 558000, P.R. China; [2]Department of Hepatology, The Third Affiliated Hospital of Sun Yat-Sen University, Guangzhou, Guangdong 510630, P.R. China; [3]Office of Scientific Research, Qiannan Medicine College for Nationalities, Duyun, Guizhou 558000, P.R. China; [4]Department of Laboratory, The People's Hospital of Qiannan, Duyun, Guizhou 558000, P.R. China

Received May 22, 2025; Accepted October 29, 2025

DOI: 10.3892/br.2026.2101

Abstract. Refractory ascites is a serious complication of decompensated cirrhosis, yet its intestinal microbial and metabolic characteristics remain incompletely understood. The present study combined 16S rRNA sequencing and gas chromatography-mass spectrometry-based untargeted metabolomics to investigate the gut microbial composition and metabolite profiles of 70 patients with refractory ascites due to cirrhosis (OB group) and 70 healthy individuals (NC group). Analyses included microbial diversity evaluation, taxonomic comparison, functional prediction, metabolite screening and disease association mapping. Compared with the NC group, the OB group showed reduced α diversity and distinct β diversity patterns, with enrichment of Proteobacteria and a reduction in anaerobic and Gram-positive taxa. BugBase analysis indicated increased proportions of potentially pathogenic, biofilm-forming and oxidative stress-tolerant phenotypes. LEfSe analysis further revealed group-specific taxa, such as enrichment of Bacteroidota and Actinobacteriota in the NC group and Firmicutes-related genera including *Clostridium* and *Lactobacillus* in the OB group. Functional predictions suggested group differences in carbohydrate and lipid metabolism, membrane transport and vitamin-related pathways. Metabolomic analysis identified 2,890 altered metabolites and Kyoto Encyclopedia of Genes and Genomes enrichment highlighted an involvement in serotonergic synapse and steroid hormone biosynthesis. Receiver operator characteristic curve analysis revealed a good discriminatory performance (area under the curve >0.93) for 10 selected metabolites. Several of these metabolites, including L-tryptophan and hypoxanthine, were further linked to inflammatory, neurodegenerative and neoplastic diseases. In conclusion, patients with refractory ascites exhibited notable structural and functional alterations in gut microbiota and metabolism. These findings provide insights into the gut-liver axis in cirrhosis and may inform future research on microbial or metabolic biomarkers.

Correspondence to: Professor Sandu Liu, Department of Hepatology, The People's Hospital of Qiannan, 9 Wenfeng Road, Duyun, Guizhou 558000, P.R. China
E-mail: liusandu@126.com

Key words: cirrhosis, refractory ascites, gut microbiota, 16S rRNA sequencing, gas chromatography-mass spectrometry metabolomics

Introduction

Refractory ascites represents a particularly severe manifestation of decompensated liver cirrhosis, often indicating a terminal disease phase marked by a diminished quality of life, frequent hospital admissions and a median transplant-free survival of only 6-12 months (1,2). Despite therapeutic advancements such as diuretic regimens, large-volume paracentesis, albumin supplementation and the use of transjugular intrahepatic portosystemic shunt (TIPS), achieving sustained symptomatic relief remains clinically challenging (3,4). Notably, accumulating evidence suggests that metabolic dysregulation persists even after TIPS, continuing to exert adverse effects on patient outcomes (5,6). In light of the limited therapeutic efficacy and marked disease burden associated with refractory ascites, there is a growing need to elucidate its underlying pathophysiological mechanisms.

Mounting research underscores the critical interplay between the gut and liver in the pathogenesis of cirrhosis (7). The intestinal microbiome, comprising a complex, adaptable microbial ecosystem, has emerged as a key regulator of hepatic homeostasis via its metabolic byproducts, immunomodulatory actions and contribution to intestinal barrier integrity (8,9). In cirrhosis, microbial dysbiosis, characterized by reduced species richness, overrepresentation of opportunistic taxa and compromised mucosal defense, is increasingly recognized as a driving factor in hepatic inflammation, bacterial translocation and secondary complications such as hepatic encephalopathy and spontaneous bacterial peritonitis (10,11). More recently, shifts in ascitic bacterial composition have been shown to correlate with disease severity and clinical prognosis, suggesting that refractory ascites may be associated with a distinct microbial signature (1,12,13). However, integrative

studies specifically addressing microbiota and metabolic alterations in this subgroup remain sparse.

Advances in high-throughput methodologies now allow for comprehensive profiling of the gut ecosystem and its metabolic outputs (14). The application of 16S rRNA sequencing in tandem with gas chromatography-mass spectrometry (GC-MS)-based untargeted metabolomics provides a multidimensional view of host-microbe interactions. A previous investigation into ascitic fluid metabolomics have highlighted notable disruptions in biochemical pathways, particularly those involved in amino acid and lipid metabolism, underscoring the metabolic complexity associated with advanced cirrhosis (15). The integration of microbial and metabolic profiling offers a promising approach to elucidate the pathophysiological mechanisms underlying refractory ascites.

In the present study, an integrated analysis of the intestinal microbiota and fecal metabolome of patients with cirrhosis-related refractory ascites was performed. Through simultaneous 16S rRNA sequencing and GC-MS-based metabolomics, the present study aimed to characterize disease-specific microbial communities and metabolic alterations. This approach may provide novel insights into the gut-liver axis disturbances contributing to disease progression and inform the development of biomarker-driven diagnostic or therapeutic strategies.

Materials and methods

Study design and participants. Between July 2023 and July 2024, a total of 140 participants were enrolled from the Department of Hepatology at Qiannan People's Hospital (Duyun, China), comprising 70 individuals clinically diagnosed with decompensated cirrhosis accompanied by refractory ascites (OB group) and 70 healthy control subjects (NC group) with comparable age and sex distribution. The age and sex distributions were as follows: in the OB group, there were 47 men and 23 women with a mean age of 59.36±10.81 years, while in the NC group, there were 24 men and 46 women with a mean age of 57.42±9.65 years. The eligible age range for inclusion was 40 to 75 years. Diagnosis of refractory ascites was established in accordance with the diagnostic criteria specified in the 2017 guidelines published by the Chinese Society of Hepatology (16). Cirrhosis in participants was diagnosed through a combination of clinical evaluations and imaging techniques, including ultrasound, CT scans and MRI. Liver biopsy was performed when necessary for confirmation, based on clinical judgment.

The NC group had no prior history of liver disease, gastrointestinal disorders or other conditions that could potentially influence the gut microbiota. Additionally, this group was not affected by chronic conditions such as hypertension, diabetes, cardiovascular issues or any ongoing inflammatory diseases. The cause of cirrhosis in participants from the OB group was established through a combination of clinical evaluation and laboratory assessments, with common underlying causes being viral hepatitis (such as hepatitis B or C virus) alcohol-related liver disease, and non-alcoholic fatty liver disease. Participants in each group were excluded if they had a history of cancer, recent abdominal surgery (particularly procedures related to the liver), uncontrolled infections or severe organ failure. Additional exclusion criteria included cachexia, recent gastrointestinal infections (within the previous month), pregnancy, lactation or the use of antibiotics, corticosteroids or probiotics within 2 weeks before enrollment.

The sample size was determined based on previous studies (17,18) with similar patient cohorts and a power analysis was conducted to ensure sufficient statistical power (80%) with a significance level of $P<0.05$ (19,20). Participants were allocated to either the OB or NC group based on predefined inclusion and exclusion criteria. The OB group included patients with confirmed cirrhosis and refractory ascites, diagnosed through clinical evaluation, imaging studies and ascitic fluid analysis. The NC group consisted of individuals without liver disease or other chronic gastrointestinal or systemic conditions and with routine laboratory test results within the normal limits. No randomization was performed for the group assignment, as this was a cohort study, but matching for age and sex between the two groups was performed. Renal function was evaluated in all OB group participants by measuring serum creatinine and calculating the glomerular filtration rate (GFR) to rule out the possibility of hepatorenal syndrome (HRS). In addition, all participants in the OB group were evaluated for the presence of hepatic encephalopathy using clinical assessment based on the West Haven criteria (21).

Upon recruitment, comprehensive dietary and lifestyle information from the previous 1 to 3 months was obtained from each subject. Dietary information was collected using a food frequency questionnaire, which asked participants about their daily food intake frequency over the past month. Lifestyle factors such as physical activity, smoking, alcohol consumption and sleep habits were assessed using self-reported surveys. These surveys covered the lifestyle of the participants in the 1 to 3 months prior to the study to account for any potential confounding factors. In the OB group, all participants underwent endoscopic evaluation to detect esophageal varices and signs of gastric bleeding, common complications in cirrhosis. Ethical approval was granted by the institutional review board of The People's Hospital of Qiannan (grant no. 2022-qnzy-18), and written informed consent was obtained from all participants prior to sample collection and data acquisition.

During the study period, no patients in the OB group experienced death directly attributable to the condition. Additionally, none of the OB group patients underwent TIPS or liver transplantation during the course of the study. All OB group patients underwent diagnostic paracentesis to determine the cause of ascites, with ascitic fluid analysis performed to assess cell count, protein concentration and albumin gradient, which was performed in accordance with the diagnostic criteria for refractory ascites as outlined in the practice guidelines by the American Association for the Study of Liver Diseases (22).

Assessment of clinical parameters. Liver function tests, including alanine aminotransferase (ALT), aspartate aminotransferase (AST), total bilirubin and albumin, were measured following standard clinical protocols. Prothrombin time (PT) and the international normalized ratio (INR) were assessed using coagulometric methods. To evaluate renal function, serum creatinine levels were determined, while urea nitrogen was measured with routine biochemical techniques. Sodium and potassium concentrations were quantified using

an automated electrolyte analyzer. The GFR was estimated using the Cockcroft-Gault formula based on serum creatinine levels (23).

Fecal sample collection and storage. Fresh fecal samples were collected from each participant, immediately snap-frozen in liquid nitrogen and then stored at -80˚C until further processing. Each sample was divided into aliquots for microbiome and metabolomic analysis, ensuring consistency and reducing freeze-thaw cycles.

Microbial DNA extraction and 16S rRNA sequencing. Genomic DNA was extracted from 200 mg of fecal material using the QIAamp Fast DNA Stool Mini Kit (Qiagen GmbH; cat. no. 51604), following the manufacturer's protocol. DNA integrity and concentration were evaluated using 1% agarose gel electrophoresis and a NanoDrop 2000 spectrophotometer. The V3-V4 hypervariable regions of the bacterial 16S rRNA gene were amplified using the primers 341F (5'-CCTACG GGNGGCWGCAG-3') and 806R (5'-GGACTACHVGGG TATCTAAT-3'), with an expected product length of ~466 bp. Amplified PCR products were purified with QIAquick PCR Purification Kit (Qiagen GmbH; cat. no. 28104) and quantified using a Qubit 3.0 fluorometer. Sequencing libraries were constructed using the TruSeq DNA PCR-Free Kit (Illumina, Inc; cat. no. 20015962). The final library concentration was quantified by qPCR and loaded at a final concentration of 12.5 nM for sequencing on the Illumina HiSeq 2500 platform. Raw reads were processed by quality filtering and paired-end merging using FLASH (v1.2.11; https://ccb.jhu.edu/software/FLASH/), followed by clustering into operational taxonomic units (OTUs) at 97% similarity using USEARCH (v1.0.667; https://www.drive5.com/usearch/). Taxonomic annotation was conducted using the Greengenes database (v13_8; https://greengenes.secondgenome.com) with a minimum confidence threshold of 0.6. α and β diversity indices (such as Chao1, Shannon and Simpson) were calculated using Quantitative Insights Into Microbial Ecology (QIIME; v1.9.1; http://qiime.org/) and MOTHUR (v1.45.3; https://mothur.org/). Principal coordinate analysis (PCoA), Bray-Curtis dissimilarity and Analysis of Similarities (ANOSIM) were performed in R (v4.3.1; https://www.r-project.org/). Functional predictions of microbial communities were generated using PICRUSt2 (v2.5.0; https://github.com/picrust/picrust2), Tax4Fun2 (v1.1.5; https://github.com/bwemheu/Tax4Fun2) and BugBase (v1.0.0; https://github.com/knights-lab/BugBase) to assess pathway involvement and phenotypic traits.

Metabolite extraction and GC-MS profiling. Fecal samples were allowed to thaw at ambient temperature before ~20 mg of each sample was transferred into a sterile 2 ml microcentrifuge tube containing 400 μl of 70% methanol with pre-added internal standards (succinic acid-D_4, cat. no. 571687; L-valine-D_8, cat. no. 486927; Sigma-Aldrich; Merck KGaA). The mixture was vortexed for 3 min to ensure adequate dispersion and then subjected to ultrasonic extraction at a frequency of 40 kHz in an ice-water bath for 10 min. After sonication, the suspension was incubated at -20˚C for 30 min to precipitate proteins and other particulates. The sample was centrifuged at 13,000 x g for 10 min at 4˚C, and 300 μl of the resulting supernatant was transferred to a new tube. A second centrifugation at 13,000 x g for 3 min was performed, after which 200 μl of the clarified supernatant was collected for downstream analysis. Untargeted metabolomic analysis was carried out using a GC-MS system (TripleTOF 6600+; SCIEX) equipped with a Waters T3 reverse-phase column (2.1x100 mm, 1.8 μm particle size). Chromatographic separation was achieved using a binary solvent system composed of 0.1% formic acid in water (mobile phase A) and 0.1% formic acid in acetonitrile (mobile phase B). The gradient program was as follows: 0 min, 95% A; 2 min, 80% A; 5 min, 40% A; 6 min, 1% A; 7.5 min, 1% A; 7.6 min, 95% A; and 10 min, 95% A. The flow rate was set at 0.4 ml/min and the injection volume was 4 μl. The column was maintained at a constant temperature of 40˚C. Mass spectrometric data were acquired in both positive and negative electrospray ionization (ESI) modes under an information-dependent acquisition method using Analyst TF 1.7.1 software (SCIEX). Ionization parameters were as follows: Ion source voltage of +5,000 V (ESI+) and -4,000 V (ESI-), source temperatures of 550˚C and 450˚C for positive and negative modes, respectively, nebulizer gas at 50 psi, auxiliary heating gas at 60 psi, curtain gas at 35 psi and a declustering potential of ±60 V. Collision energies were set at ±10 V for MS1 and ±30 V for MS2, with a collision energy spread of 15 V. Each mode was acquired over a total runtime of 10 min. The present study employed an untargeted metabolomics approach and data were acquired in full-scan mode. Metabolite identification was based on matching retention times and mass spectra with those in the NIST and Fiehn libraries (see below).

Metabolomic data processing. Raw data obtained from GC-MS analysis were initially processed using ChromaTOF software (v.4.72; LECO Corporation) for peak detection, deconvolution and retention time alignment. Baseline correction and noise filtering were applied to enhance signal clarity and ensure consistent feature extraction. Metabolic features with >50% missing values across all samples were excluded from further analysis. The remaining missing values were estimated using a k-nearest neighbor algorithm to maintain data completeness without compromising structure. To account for instrument drift and technical variability, total ion current normalization was applied across all chromatograms. Compound identification was performed by matching deconvoluted spectra against commercial reference libraries, such as NIST (https://www.nist.gov/srd/nist-standard-reference-database-1a) and FiehnLib (https://fiehnlab.ucdavis.edu/projects/fiehnlib), using a similarity threshold of ≥80%. Metabolite identities were further verified through manual inspection of fragmentation patterns and retention indices. Only compounds consistently detected in the quality control samples with a coefficient of variation <30% were retained for downstream statistical analysis. All post-processing, normalization and compound filtering, as well as the subsequent multivariate and univariate analyses, were performed in MetaboAnalyst 5.0 (https://www.metaboanalyst.ca). Data transformation and scaling were applied within the platform prior to these statistical analyses. The diagnostic efficiency of differential metabolites was evaluated by constructing receiver operating characteristic (ROC) curves in R (v.4.3.0) with the pROC package, and the area under the

curve (AUC) was calculated to quantify their discriminative ability.

Functional enrichment analysis. Metabolites retained after annotation and filtering were mapped to reference pathways based on the Kyoto Encyclopedia of Genes and Genomes (KEGG) compound database. Functional enrichment analysis was conducted using the KEGG Pathway platform (https://www.genome.jp/kegg/), aiming to identify significantly perturbed metabolic routes across experimental conditions. Enrichment significance was evaluated based on the hypergeometric test, with a false discovery rate cut-off of <0.05 used to define significantly enriched pathways. Pathway coverage and biological relevance were also considered in the final interpretation. In addition, associations between key metabolites and human diseases were explored using the Human Metabolome Database (HMDB; https://hmdb.ca/).

Statistical analysis. Statistical procedures were used to compare microbial and metabolomic characteristics between groups and to assess their relationships with clinical variables. For microbiome data, differences in α-diversity were evaluated using either parametric or non-parametric tests, selected according to the distribution of the data with unpaired Student's t-test applied to normally distributed data and the Wilcoxon rank-sum test used for non-normally distributed data. For examining individual metabolite differences in the metabolomic data, appropriate univariate tests were used depending on data distribution, including unpaired Student's t-test or the Wilcoxon rank-sum test. Only metabolites that met the predefined criteria for statistical significance were included in subsequent interpretation. Associations between refractory ascites and clinical indicators were examined using Pearson correlation analysis. GraphPad Prism (version 9.5.1; Dotmatics) was used for these statistical analyses. $P<0.05$ was considered to indicate a statistically significant difference.

Results

Patients in the OB group have reduced microbial richness and diversity. A total of 749 OTUs were obtained following rigorous quality filtration and sequence clustering of 16S rRNA gene reads. Among them, 572 OTUs were identified in the NC group and 540 in the OB group, with 363 OTUs shared across both cohorts. The Venn diagram illustrates the distribution of overlapping and group-specific OTUs (Fig. 1A). To further characterize the pattern of taxa presence and co-occurrence, an UpSet plot was constructed. The plot provided a more granular view of intersection sets and subgroup relationships (Fig. 1B). This visualization offered an intuitive overview of OTU overlap and structural complexity between the groups. To assess within-sample microbial diversity, α diversity indices were calculated and compared between the groups. As shown in Fig. 1C, richness estimators, including Ace, Chao1 and Sobs, were significantly lower in the OB group than in the NC group ($P<0.05$), indicating a marked reduction in microbial richness. Similarly, Shannon and Simpson indices were decreased in the OB group, reflecting diminished community evenness and overall diversity compared with the NC group. Notably, the Coverage index approached 1 in both groups, confirming sufficient sequencing depth and reliable representation of microbial communities.

Additionally, clinical parameters of the NC and OB groups were analyzed. The results indicated that in the OB group, liver function markers (ALT, AST and total bilirubin) were higher, albumin was lower, coagulation markers (prothrombin time and INR) were prolonged, creatinine levels were elevated and electrolyte concentrations (sodium and potassium) were lower. No significant change was observed in urea nitrogen levels (Table I). These findings reflected a decline in microbial richness and diversity in individuals with refractory ascites, highlighting notable ecological disturbance associated with cirrhosis.

β diversity analysis reveals distinct microbial community structures between the OB and NC groups. To evaluate the structural variation of the gut microbiota between cirrhotic patients and healthy individuals, β diversity analysis was performed across multiple taxonomic levels. PCoA plots based on Bray-Curtis distances revealed a clear spatial separation between the NC and OB groups at all six taxonomic ranks, from phylum to species (Fig. 2A), indicating distinct community compositions between the groups. The degree of separation appeared more pronounced at lower taxonomic levels, particularly at the genus and species ranks. The ANOSIM results further supported these observations, demonstrating significant dissimilarities between groups at each taxonomic rank (Fig. 2B; $r>0.25$, $P<0.001$). Together, these findings illustrate that the gut microbial communities of cirrhotic patients differed markedly from those of healthy controls, suggesting ecological shifts linked to disease progression.

Functional and phenotypic alterations of gut microbiota in the OB group. Next, the potential functional differences in the gut microbiota between groups was explored. Microbial gene functions were inferred using PICRUSt2. As displayed in Fig. 3A, the pathways related to 'Carbohydrate Metabolism,' 'Membrane Transport' and the 'Metabolism of Cofactors and Vitamins' were among the most notable predicted functions, with observable differences noted between the NC and OB samples. Several immune- and disease-related pathways, such as those associated with infectious diseases, neurodegenerative disorders and endocrine system regulation, also displayed significant variation. Additionally, microbial phenotypic characteristics were analyzed using BugBase (Fig. 3B and C). The heatmap revealed contrasting trends in phenotypes such as aerobicity, pathogenic potential and biofilm formation between the two cohorts. Quantitative comparisons showed that compared with the NC group, the OB group exhibited higher proportions of 'Aerobic', 'Contains_Mobile_Elements', 'Facultatively_Anaerobic', 'Forms_Biofilms', 'Gram_Negative', 'Potentially_Pathogenic' and 'Stress_Tolerant' phenotypes. By contrast, the 'Anaerobic' and 'Gram_Positive' phenotypes were significantly lower in the OB group (Fig. 3C). These findings suggest that microbial functional capacities and phenotype expression profiles were altered in the OB group, as reflected by distinctions in the predicted pathways and microbial traits.

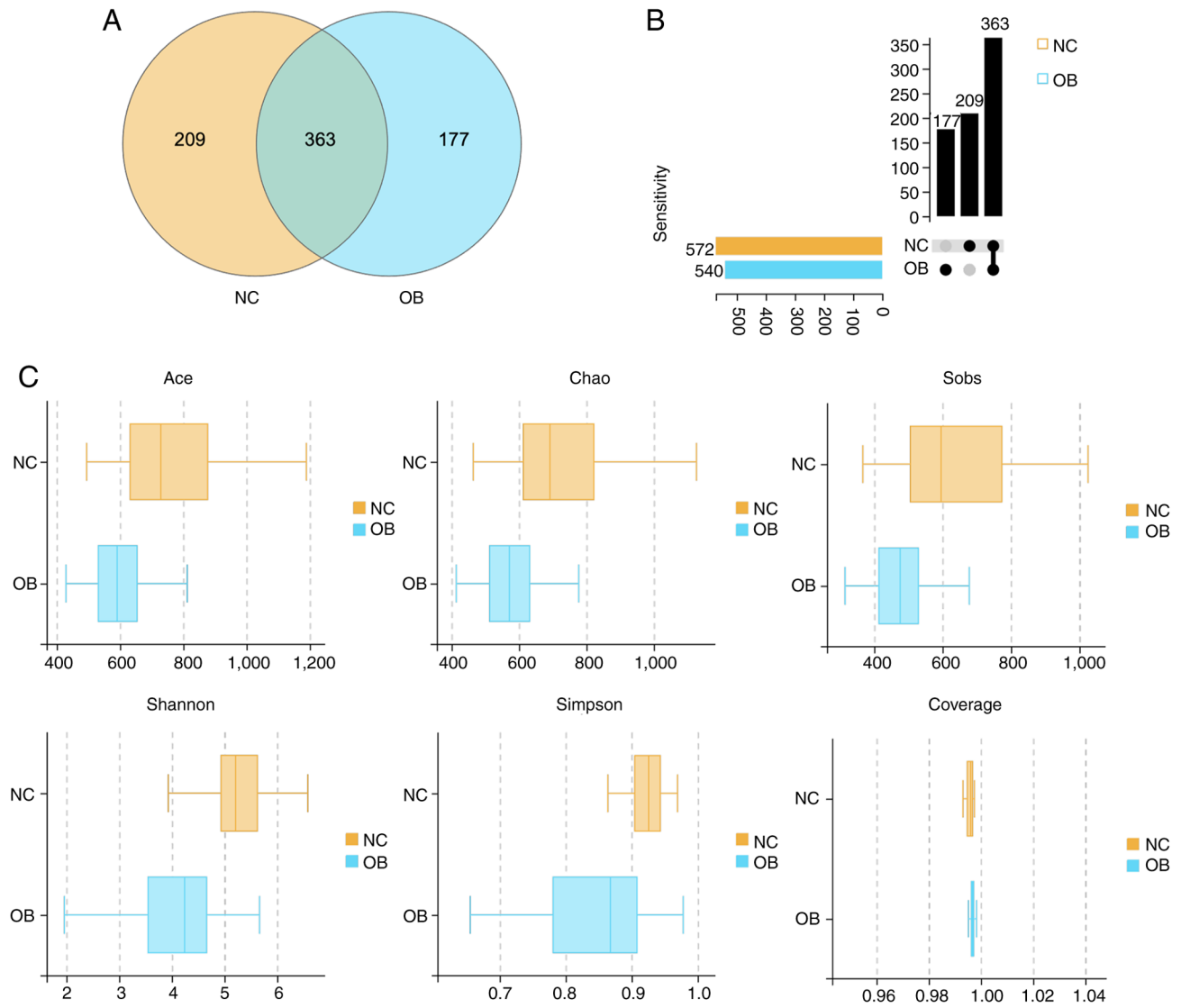

Figure 1. OTU comparison and α diversity profiling of intestinal microbiota between the NC and OB groups. (A) Venn diagram illustrating the number of shared and unique OTUs in each group. (B) UpSet plot depicting the distribution and intersection patterns of OTUs across the two cohorts. (C) Boxplots of α diversity indices (Ace, Chao1, Sobs, Shannon, Simpson and Coverage) comparing species richness and microbial community diversity between the NC and OB groups. OTU, operational taxonomic unit; NC, normal control; OB, refractory ascites group.

Microbial taxa with differential distribution identified by LEfSe. To investigate the taxonomic differences in gut microbiota composition between the OB and NC groups, LEfSe analysis was performed to identify taxa exhibiting differential abundance across taxonomic ranks. The cladogram in Fig. 4A illustrates the phylogenetic structure of these taxa, with color-coded branches representing features associated with either the NC or OB group. Several taxa were found to vary in relative abundance between groups (Fig. 4B). For instance, members of the phyla Bacteroidota and Actinobacteriota appeared more associated with the NC group, while taxa belonging to Firmicutes, including genera such as *Clostridium* and *Lactobacillus*, were relatively more abundant in the OB group. These variations were evident across multiple levels of taxonomy, suggesting distinct microbial profiles characterizing the two cohorts.

Metabolomic distinctions between the OB and NC groups based on GC-MS analysis. Building on the observed taxonomic differences in gut microbiota, untargeted metabolomic profiling was performed to investigate compositional variations at the metabolite level. Fecal samples from both the OB and NC groups were analyzed using GC-MS and the representative total ion chromatograms showed comparable spectral patterns across samples (Fig. 5A). PCA based on the full metabolite dataset revealed a distributional shift between the OB and NC groups (Fig. 5B), with samples from each cohort forming distinguishable clusters. This suggests divergence in global metabolic features between the two groups. Differential metabolite screening further identified a wide array of altered features. A total of 8,777 metabolites were detected, among which 1,334 exhibited increased abundance and 1,556 were decreased in the OB group compared with the NC group (Fig. 5C). To highlight the most relevant metabolic shifts, the top 20 upregulated and downregulated metabolites based on fold change and P-value are summarized in Tables II and III, respectively. These tables provide detailed chemical information, statistical significance and fold changes of the most altered compounds, thereby offering a clearer view of the

Table I. Clinical parameters comparisons between the OB and NC groups.

Clinical parameter	NC group (n=70)	OB group (n=70)	P-value
Sex, male/female	24/46	31/39	0.84
Liver function tests			
ALT, U/l	24.71±1.15	52.27±6.54	0.0002
AST, U/l	23.04±1.04	134.57±23.16	<0.001
Total bilirubin, μmol/l	17.07±2.36	61.41±9.51	<0.001
Albumin (g/l)	48.18±0.46	29.64±1.09	<0.001
Coagulation function			
Prothrombin time, sec	12.64±0.11	17.39±0.31	<0.001
International normalized ratio	1.18±0.01	1.45±0.03	<0.001
Renal function			
Creatinine, μmol/l	66.47±1.33	133.62±21.67	<0.001
Urea nitrogen, mmol/l	5.88±0.18	7.87±0.66	0.1378
Electrolytes			
Sodium, mmol/l	140.76±0.37	137.51±0.58	<0.001
Potassium, mmol/l	4.36±0.06	4.00±0.08	<0.001

OB, refractory ascites group; NC, negative control; ALT, alanine aminotransferase; AST, aspartate aminotransferase.

molecular disturbances associated with the OB group. These results offer an initial view of metabolic alterations between the OB and NC groups.

Exploration of enriched pathways linked to altered metabolites. Based on the screened differential metabolites, a compound network was constructed to illustrate chemical associations and structural classifications. Metabolites were categorized into groups such as amino acid derivatives, steroids, fatty acids and heterocyclic compounds, with dense interconnections observed both within and between chemical classes (Fig. 6A). Then, KEGG pathway enrichment was conducted using the annotated metabolites. A range of pathways were implicated, including those involved in neurotransmitter signaling (such as 'Serotonergic synapse'), lipid metabolism (such as 'Fatty acid biosynthesis' and 'Fatty acid degradation') and hormonal regulation (such as 'Steroid hormone biosynthesis' and 'Oxytocin signaling pathway') (Fig. 6B).

Evaluation of diagnostic performance of differential metabolites. The present study further assessed the classification potential of key metabolites with receiver operator characteristic curve analysis. A total of 10 representative metabolites were selected based on their relevance in prior screening and annotation. All selected metabolites yielded area under the curve (AUC) values ≥0.93, with the highest observed for 6-ketoprostaglandin E1 (AUC=0.955). Other compounds such as prostaglandin D3 (AUC=0.940), deoxyartemisinin (AUC=0.937) and ganoderic acid Md (AUC=0.930) also exhibited strong classification performance. The full list included: biotin-XX-hydrazide (AUC=0.936), estra-4,9-diene-3,17-dione (AUC=0.933), prostaglandin E2 methyl ester (AUC=0.931), 8-epidermal glycoside (AUC=0.930), pergolide (AUC=0.930) and cincassiol B (AUC=0.930) (Fig. 7). These results suggest that the identified features may have contributed to group differentiation in the metabolomics cohort and provide reference for subsequent validation efforts.

Disease association of key differential metabolites. Beyond evaluating the diagnostic value of the differential metabolites, their potential links to human diseases were further investigated by referencing the KEGG and HMDB databases. Among them, L-tryptophan, hypoxanthine, and indole exhibited broad associations with various pathological conditions, notably encompassing neurological disorders (such as epilepsy, schizophrenia and Alzheimer's disease), chronic inflammatory diseases (including Crohn's disease, ulcerative colitis and rheumatoid arthritis), as well as multiple malignancies (such as colorectal, ovarian and pancreatic cancer). For example, L-tryptophan alone was associated with >20 disease states, reflecting its multifaceted role in systemic metabolic regulation. Likewise, hypoxanthine was associated with several metabolic syndromes and tumor-related processes. Besides, other metabolites, including serotonin, phenylethylamine and deoxycholic acid, were implicated in both gastrointestinal and neuropsychiatric conditions (Table IV). Collectively, these associations underscored the potential involvement of these metabolites in disease-related metabolic pathways and support their biological relevance within the study context.

Correlation between refractory ascites and clinical parameters. To further explore the clinical relevance of refractory ascites, Pearson correlation analysis was performed between refractory ascites status and routine clinical parameters. The results demonstrated that refractory ascites was positively correlated with PT (r=0.536, P<0.001), INR (r=0.533, P<0.001), TBIL (r=0.384, P=0.001) and urea nitrogen (r=0.285, P=0.019), while showing negative correlations with serum

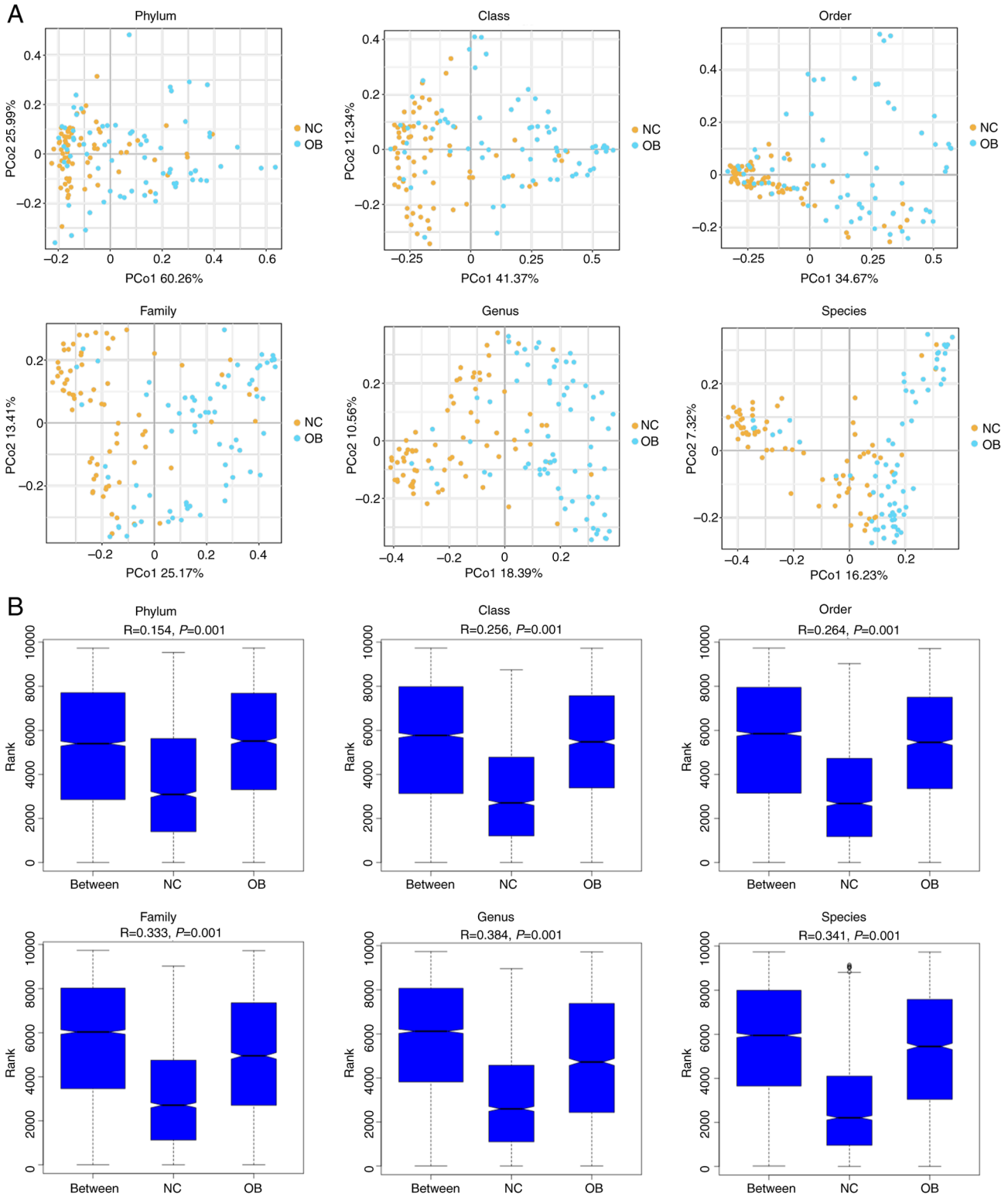

Figure 2. β diversity analysis of intestinal microbiota between the NC and OB groups. (A) PCoA plots based on Bray-Curtis distances were generated across six taxonomic ranks: Phylum, class, order, family, genus and species. (B) Analysis of Similarities compared intragroup and intergroup microbial distances at each taxonomic level. NC, normal control; OB, refractory ascites group; PCoA, principal coordinates analysis.

albumin (r=-0.299, P=0.012) and sodium (r=-0.270, P=0.024). No significant associations were observed with age, sex, ALT, AST, potassium or creatinine (all P>0.05). These findings suggest that impaired coagulation, hyperbilirubinemia, hypoalbuminemia and electrolyte or renal disturbances are closely linked with the presence of refractory ascites (Table V).

Discussion

The present study offers an in-depth and integrative assessment of microbial dysbiosis and metabolic abnormalities in individuals with refractory ascites secondary to cirrhosis, uncovering notable disturbances across the gut-liver axis.

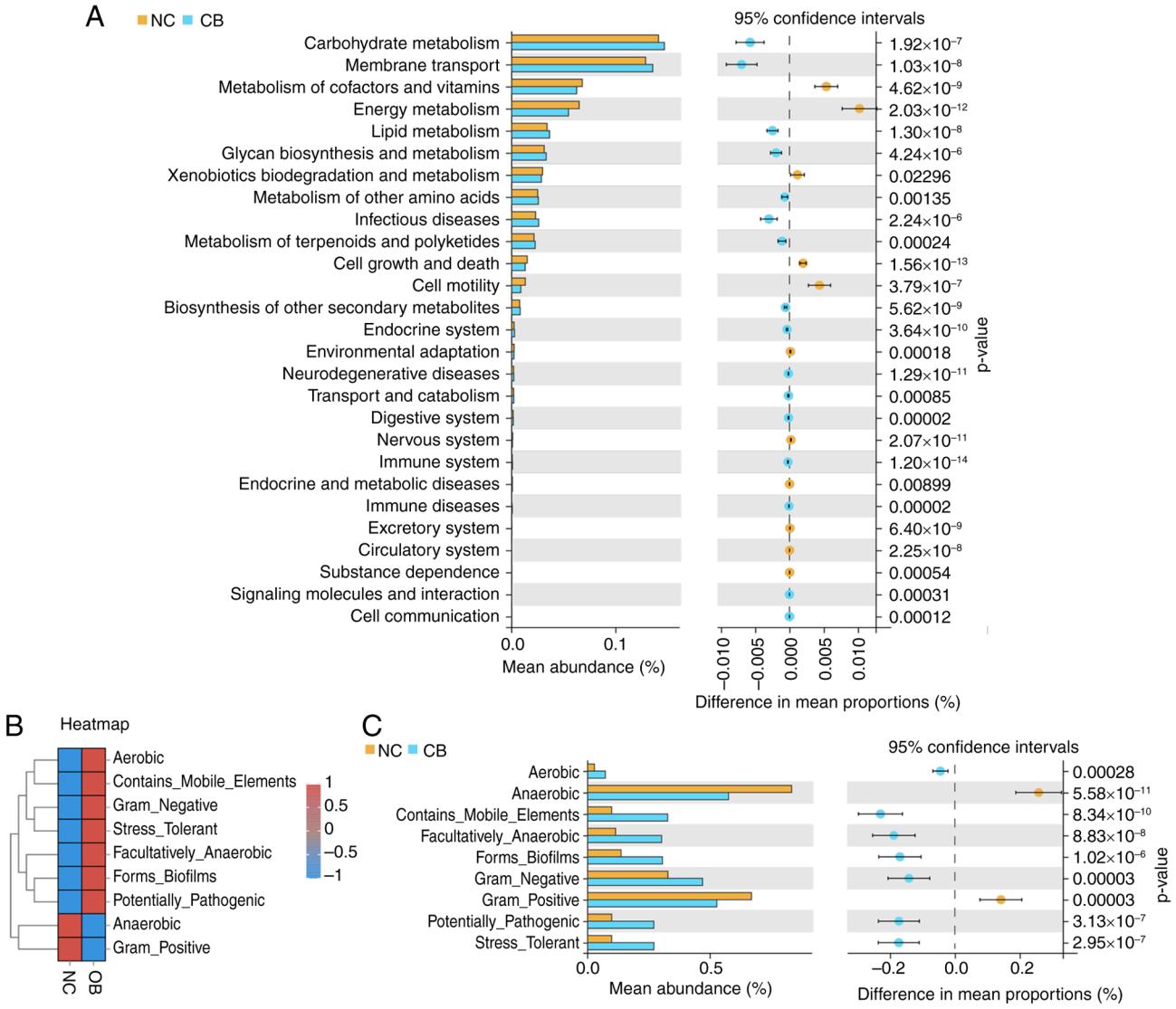

Figure 3. Functional and phenotypic characterization of intestinal microbiota in the NC and OB groups. (A) Kyoto Encyclopedia of Genes and Genomes pathway enrichment predicted by PICRUSt2 presented relative abundances and statistical differences between the two groups. (B) BugBase-derived heatmap illustrated the distribution patterns of microbial phenotypes across the NC and OB samples. (C) Selected microbial phenotypes predicted by BugBase were compared between the groups. NC, normal control; OB, refractory ascites group.

The data revealed a marked decline in intestinal microbial richness and significant compositional divergence between the refractory ascites cohort and healthy counterparts. These alterations included a notable proliferation of Proteobacteria, particularly Enterobacteriaceae, alongside a depletion of beneficial anaerobes such as Bacteroidota and Actinobacteriota. Such microbial transitions favoring pathogenic species with enhanced oxidative resilience and biofilm-forming capacities may aggravate bacterial translocation and systemic inflammatory responses, both central to the disease pathophysiology.

In the present study, 16S rRNA sequencing was employed to characterize the microbial community structure, a high-throughput and widely validated approach that targets the variable regions of bacterial ribosomal RNA genes to resolve taxonomic profiles (24). This technique has been extensively utilized across diverse clinical contexts, including gastrointestinal, hepatic and respiratory diseases (25-28). For instance, it has been applied to identify nasopharyngeal microbiota alterations in SARS-CoV-2 infection (29). Although widely used in cirrhosis research, its specific application in the context of refractory ascites remains underrepresented. This technique enables the detection of nuanced but clinically meaningful shifts that would likely be missed through conventional culture methods (30,31). In addition to overall compositional shifts, distinct dominance patterns in the OB group were identified in the present study, with taxa such as Escherichia-Shigella, Enterobacteriaceae and Gammaproteobacteria markedly enriched compared with controls. These microbial signatures may reflect selective pressures favoring opportunistic pathogens under cirrhotic gut conditions. The use of 16S rRNA gene sequencing, a more specific approach than traditional cultures, enabled the resolution of taxonomic profiles with greater precision in the present study. However, we acknowledge that while this method offers significant advantages in microbial identification, challenges remain in terms of both the cost and the systematic application of metabolite studies in clinical settings. Future research

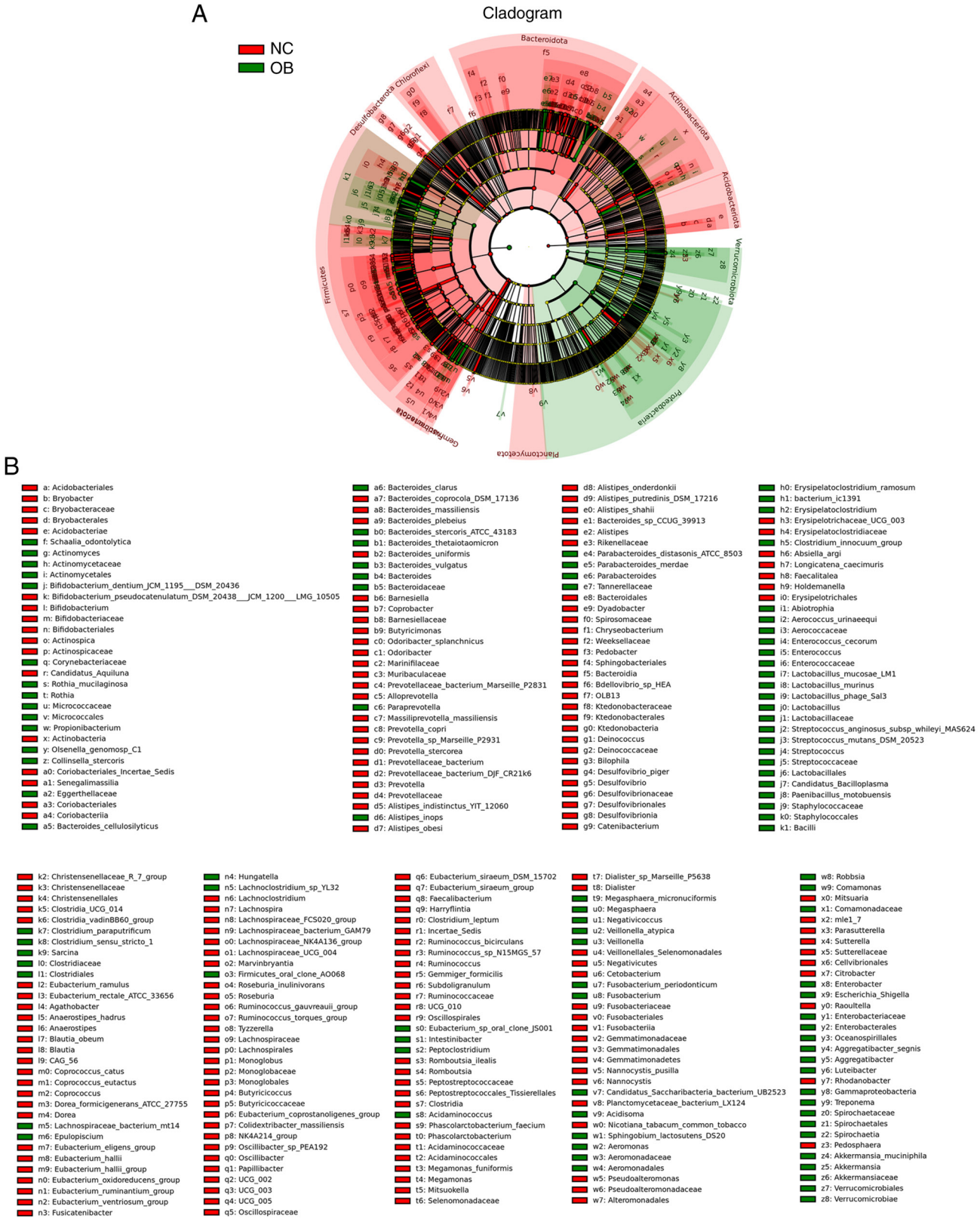

Figure 4. Differential taxonomic features of intestinal microbiota identified by LEfSe analysis between the NC and OB groups. (A) A taxonomic cladogram was constructed using LEfSe to visualize the phylogenetic distribution of taxa differing in relative abundance between the two groups, spanning from the phylum to the genus level. (B) Corresponding list of significantly enriched taxa, with red indicating enrichment in NC and green indicating enrichment in OB. NC, normal control; OB, refractory ascites group.

may need to explore ways to reduce the cost of metabolite studies and promote their standardization, ensuring broader applicability in clinical practice.

Findings from BugBase phenotype predictions substantiated the observations of the present study, indicating elevated levels of Gram-negative bacteria, facultative anaerobes

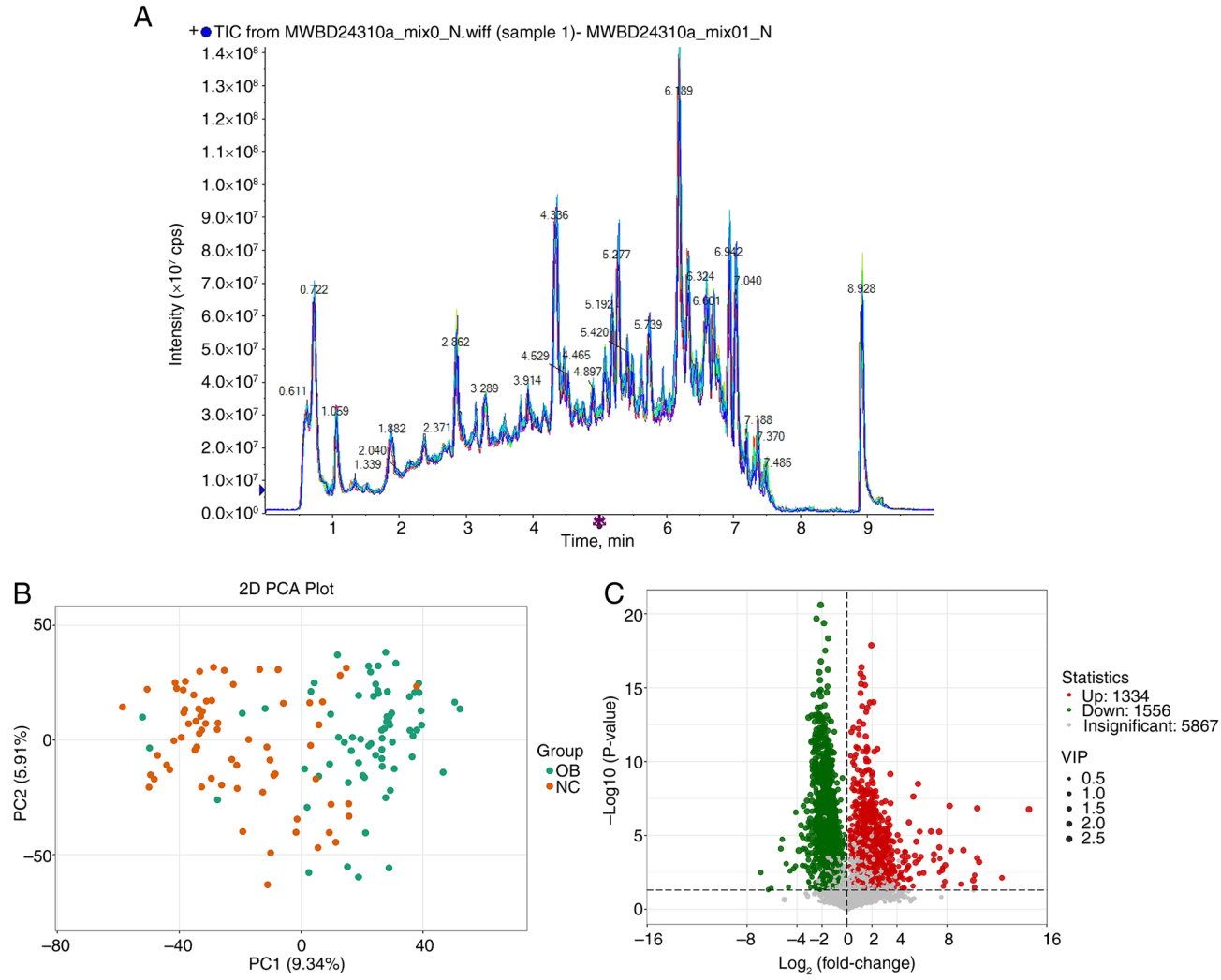

Figure 5. Untargeted fecal metabolomic profiling using GC-MS of the NC and OB groups. (A) Total ion chromatograms from representative fecal samples were obtained through GC-MS (an asterisk at 5 min indicates the internal alignment marker). (B) PCA based on global metabolite features revealed distinct clustering patterns between the NC and OB groups, suggesting underlying differences in metabolic composition. (C) A volcano plot was used to present the distribution of differential metabolites. NC, normal control; OB, refractory ascites group; GC-MS, gas chromatography-mass spectrometry; PCA, principal component analysis; cps, counts per sec; VIP, variable importance in projection.

and organisms capable of biofilm production in the ascitic group. These insights are consistent with recent work by Shi *et al* (32), who utilized metagenomic next-generation sequencing (mNGS) to reveal a high prevalence of polymicrobial infections in cirrhotic ascitic fluid, including a dominance of Enterobacteriaceae and other fastidious facultative pathogens not detected via traditional culture techniques. Their conclusions emphasized the pathogenic potential of microbial imbalances and invasive phenotypes in precipitating spontaneous bacterial peritonitis and systemic immune activation (32), thereby reinforcing the clinical significance of the microbiota-based findings of the present study. Notably, these pathogenic phenotypes also suggest that hypoxia-induced niche disruption and accumulation of oxidative stress-tolerant species may be key contributors to intestinal permeability, further linking microbial dysfunction with systemic disease progression.

In the present study, further functional inference revealed disruptions in microbial pathways governing carbohydrate metabolism, vitamin biosynthesis and membrane-associated transport systems. These imbalances may hinder the production of beneficial microbial metabolites, such as short-chain fatty acids, and compromise host mucosal defense. Similar host-microbiota interactions have been reported in colitis models, where Marinifilaceae enrichment was linked to suppressed cell cycle signaling in Toll-like receptor 2-deficient mice (33). Comparable disruptions have been described by Gitto *et al* (34), who observed persistent functional impairments in gut microbiota among patients post-TIPS procedure, including reduced synthesis of anti-inflammatory lipids such as octanoic acid and enrichment of inflammation-promoting taxa. While their study focused on post-intervention systemic effects, the results of the present study highlight the possibility that such microbial dysregulation originates earlier at the intestinal level. The integration of functional annotation tools with community structure analysis in the present study provides enhanced mechanistic insight.

In parallel, comprehensive untargeted metabolite profiling using GC-MS, a technique renowned for its sensitivity in detecting low-molecular-weight volatile and semi-volatile

Table II. Top 20 upregulated differential metabolites between the OB and NC groups.

No.	Compound	Formula	P-value	Log2FC
1	4-Chloro-5-sulfamoylanthranilic acid	$C_7H_7C_lN_2O_4S$	<0.0001	14.58
2	Lithospermic acid B	$C3_6H_{30}O_{16}$	0.0075	12.41
3	Dihydrorobinetin	$C_{15}H_{12}O_7$	0.0006	10.58
4	2,8-Dichloro-3-dibenzofuranol	$C_{12}H_6C_{12}O_2$	<0.0001	10.43
5	Diflunisal	$C_{13}H_8F_2O_3$	0.0003	10.42
6	S1P Lyase Fluorogenic Substrate	$C_{15}H_{10}O_8S$	0.0330	10.21
7	[3-(6,7-dihydroxy-4-oxo-4H-chromen-2-yl) phenyl] oxidanesulfonic acid	$C_{14}H_{10}C_lN_3O_4S$	0.0109	10.11
8	N-[(3-chloro-2-hydroxy-5-nitrophenyl) carbamothioyl] benzamide	$C_6H_{11}O_6PS$	0.0001	9.32
9	5-(Methylthio)-2,3-dioxopentyl phosphate	$C_{19}H_{12}O_8$	0.0001	8.32
10	(1R*,3R*,3'S*)-1,2,3,4-Tetrahydro-1-(2-thio-3-pyrrolidinyl)-beta-carboline-3-carboxylic acid	$C_8H_7C_lN_4S$	<0.0001	8.21
11	Diacerein	$C_{15}H_{11}C_lN_2O_2$	0.0010	7.86
12	6-(2-Chloroallylthio)purine	$C_{40}H_{40}O_{11}$	0.0135	7.83
13	Oxazepam	$C_{14}H_{12}O_6S$	0.0271	7.72
14	1-[3-(6-{2,4-dihydroxy-3-[(1E)-3-methylbut-1-en-1-yl] benzoyl}-5-(2,4-dihydroxyphenyl)-4-hydroxy-3-methylcyclohex-2-en-1-yl)-2,4-dihydroxyphenyl]-3-(2,4-dihydroxyphenyl) propan-1-one	$C_{13}H_{19}N_3O_{10}$	0.0016	7.66
15	Resveratrol-3-O-sulfate	$C_{23}H_{34}O_5$	0.0023	7.62
16	Glu-Asp-Asp	$C_{18}H_{14}O_8$	0.0004	7.44
17	Latanoprost acid	$C_{36}H_{28}O_{16}$	0.0032	7.4
18	(2S-3S)-versiconal hemiacetal	$C_{12}H_{11}C_lN_2O_5S$	0.0001	7.39
19	Theaflavin monogallates	$C_{16}H_{30}N_4O_5$	<0.0001	7.39
20	Furosemide	$C_{23}H3_1FO_6$	0.0002	6.96

OB, refractory ascites group; NC, negative control; FC, fold change.

compounds, was performed in the present study. GC-MS has garnered increasing attention in hepatology due to its ability to delineate metabolic signatures indicative of liver pathology and ascitic fluid composition (15,35). In the present study, fecal metabolomics allowed the identification of gut-derived biochemical alterations, a number of which were associated with the observed microbiome shifts. Notably, compared with ascitic fluid-based metabolomics, fecal analysis may offer earlier and more direct insights into intestinal metabolic dysfunctions that precede systemic involvement, such as peritonitis or encephalopathy (36).

In the present study, an integrative metabolomic analysis combining GC-MS and LC-MS platforms uncovered ~2,900 differentially expressed fecal metabolites. KEGG pathway enrichment analysis revealed significant disturbances in serotonergic synapse activity, steroid biosynthesis and neuroactive ligand-receptor signaling networks. These findings mirror those of Beyoğlu *et al* (15), who reported increased amino acid levels and reduced fatty acid content in ascitic fluid from cirrhotic patients, pointing to malabsorption and lipid processing failure. Metabolites such as L-tryptophan and hypoxanthine, consistently elevated in both the present study and the study by Beyoğlu *et al* are recognized modulators of immune and neurological function (37,38). Additionally, the present study identified gut-origin compounds, such as indole and deoxycholic acid, which may serve as intermediaries in gut-liver communication pathways and merit further mechanistic exploration.

Sustained oxidative stress is widely acknowledged as a defining feature of advanced-stage liver cirrhosis, where it contributes to the disruption of epithelial integrity, propagation of systemic inflammation and dysregulation of immune responses (39,40). Within this pathological framework, multiple metabolites uncovered in the present study, including hypoxanthine, deoxycholic acid and several indole-related molecules, appear to engage in redox-sensitive processes and ROS-driven signaling cascades (41-43). These metabolites not only mirror the prevailing oxidative imbalance but may also functionally reinforce inflammatory pathways and enhance intestinal permeability. Their consistent elevation in fecal profiles of patients with refractory ascites reinforces their biological relevance and suggests utility as molecular tracers of gut-liver axis dysfunction. Among the metabolite features showing significant differential expression in the present study, 10 exhibited outstanding discriminatory accuracy (AUC≥0.93), indicating promising diagnostic

Table III. Top 20 downregulated differential metabolites between the OB and NC groups.

No.	Compound	Formula	P-value	Log2FC
1	Cortisone acetate	$C_{23}H_{30}O_6$	0.0033	-6.90
2	Colubrinic acid	$C_{30}H_{46}O_4$	0.0470	-6.30
3	2-[1-Hydroxy-3-(4-methoxyphenyl)propyl]-3,5-dimethoxyphenol	$C_{18}H_{22}O_5$	0.0379	-6.06
4	Goshonoside F2	$C_{26}H_{44}O_8$	0.0001	-5.30
5	Fasciculic acid C	$C_{38}H_{63}NO_{11}$	<0.0001	-5.18
6	Imperialine	$C_{27}H_{43}NO_3$	0.0008	-4.86
7	Lys-Lys-Ser	$C_{15}H_{31}N_5O_5$	0.0315	-4.68
8	Glu-Gln-Gln	$C_{15}H_{25}N_5O_8$	0.0026	-4.56
9	Sarpagine	$C_{19}H_{22}N_2O_2$	0.0018	-4.28
10	(Z)-7-[(2R)-3-hydroxy-2-[(E,4R)-4-hydroxy-4-(1-propylcyclobutyl) but-1-enyl]-5-oxocyclopentyl]hept-5-enoic acid	$C_{23}H_{36}O_5$	0.0012	-4.12
11	Isoeugenitol	$C_{11}H_{10}O_4$	<0.0001	-4.09
12	Prostaglandin E2 methyl ester	$C_{21}H_{34}O_5$	0.0001	-3.86
13	(1R,8S,9S)-3,4-dihydroxy-8-methoxy-11,11-dimethyl-5-propan-2-yl-16-oxatetracyclo[7.5.2.01,10.02,7]hexadeca-2,4,6-trien-15-one	$C_{21}H_{28}O_5$	<0.0001	-3.69
14	E-Norendoxifen	$C_{24}H_{25}NO_2$	<0.0001	-3.65
15	Oleyl acetate	$C_{20}H_{38}O_2$	0.0011	-3.56
16	Val-Asp-Asp	$C_{13}H_{21}N_3O_8$	<0.0001	-3.54
17	14,15-Epoxyemindole SB	$C_{28}H_{39}NO_2$	0.0001	-3.52
18	Phe-Ile-His-Arg	$C_{27}H_{41}N_9O_5$	<0.0001	-3.48
19	Tiocarlide	$C_{23}H_{32}N_2O_2S$	0.0012	-3.34
20	Fingolimod	$C_{19}H_{33}NO_2$	0.0001	-3.32

OB, refractory ascites group; NC, negative control; FC, fold change.

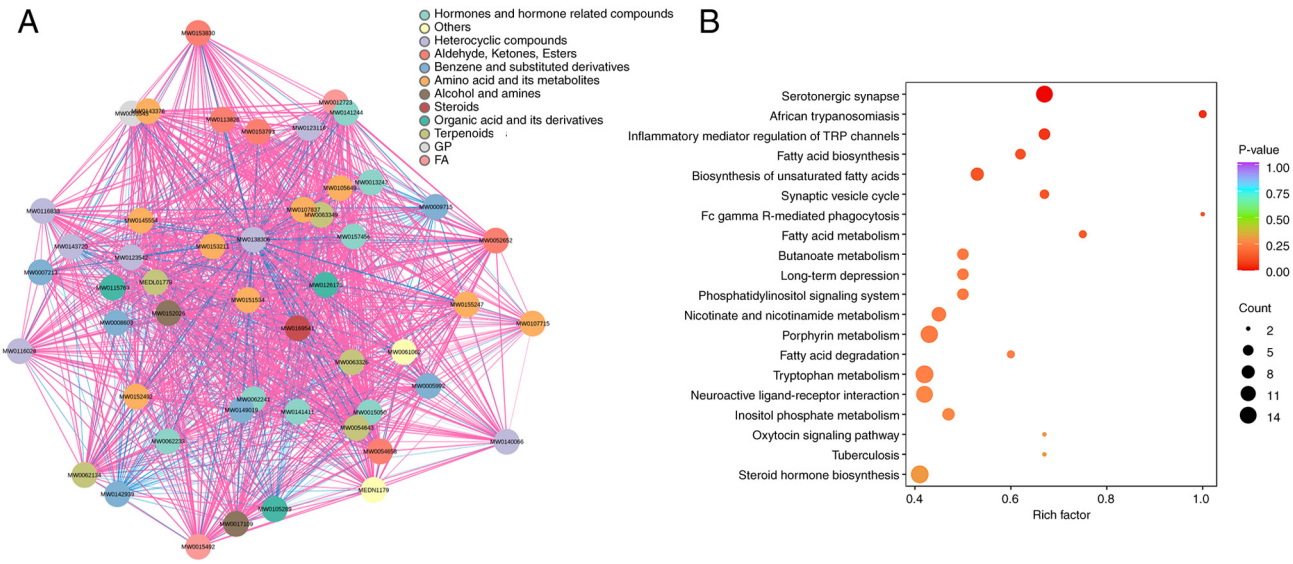

Figure 6. Functional interpretation of differential metabolites through network construction and KEGG pathway enrichment. (A) A compound interaction network was constructed based on chemical similarity and classification, with node colors representing distinct metabolite categories. (B) KEGG enrichment analysis was performed on the identified metabolites. KEGG, Kyoto Encyclopedia of Genes and Genomes.

applicability. These molecular indicators could complement existing clinical practices for the early identification and stratification of refractory ascites cases. Building upon prior findings by Beyoğlu *et al* (15), the present study contributes additional gut-associated candidates with putative roles in modulating redox homeostasis, host metabolism and immune signaling dynamics.

Unlike prior investigations that often analyzed microbial or metabolomic dimensions in isolation, the present study employed a dual-omics strategy to uncover co-occurring

Table IV. Disease associations of differential metabolites: Refractory ascites groups vs. healthy group.

Compound Name	The Human Metabolome Database diseases
L-Tryptophan	Epilepsy | Schizophrenia | Alzheimer's disease | Colorectal cancer | Ovarian cancer | Obesity | Nicotinamide adenine dinucleotide deficiency | Hartnup disease | Leukemia | Olivopontocerebral atrophy | Hereditary spastic paraplegia | Hypothyroidism | Friedreich's ataxia | Celiac disease | Irritable bowel syndrome | Ulcerative colitis | Autism | Crohn's disease | Rheumatoid arthritis | Perillyl alcohol administration for cancer treatment | Pancreatic cancer | Periodontal disease | Frontotemporal dementia | Lewy body disease | Attachment loss | Periodontal probing depth | Cachexia | Eosinophilic esophagitis | Tryptophanuria with dwarfism
Hypoxanthine	Lesch-Nyhan syndrome | Canavan disease | Thymidine treatment | Uremia | Xanthinuria type 1 | Degenerative disc disease | Hydrocephalus | 3-methyl-crotonyl-glycinuria | Irritable bowel syndrome | Colorectal cancer | Crohn's disease | Ulcerative colitis | Rheumatoid arthritis | Perillyl alcohol administration for cancer treatment | Pancreatic cancer | Periodontal disease | Alzheimer's disease | Frontotemporal dementia | Lewy body disease | Attachment loss | Periodontal probing depth | Lung cancer | Autosomal dominant polycystic kidney disease | Eosinophilic esophagitis | Hepatocellular carcinoma | Molybdenum cofactor deficiency | Sulfite oxidase deficiency, ISOLATED | Phosphoribosylpyrophosphate synthetase superactivity
Tryptamine	Irritable bowel syndrome | Colorectal cancer
Phenethylamine	Bulimia nervosa | Crohn's disease | Ulcerative colitis | Minimal brain dysfunction | Autism
Nicotinic acid	Alcoholism | Colorectal cancer | Crohn's disease | Ulcerative colitis | Attachment loss | Missing teeth | Periodontal probing depth
7-Methylguanine	Colorectal cancer
Deoxycholic acid	Cystic fibrosis | Irritable bowel syndrome | Ulcerative colitis | Colorectal cancer | Primary biliary cirrhosis
Oxindole	Colorectal cancer

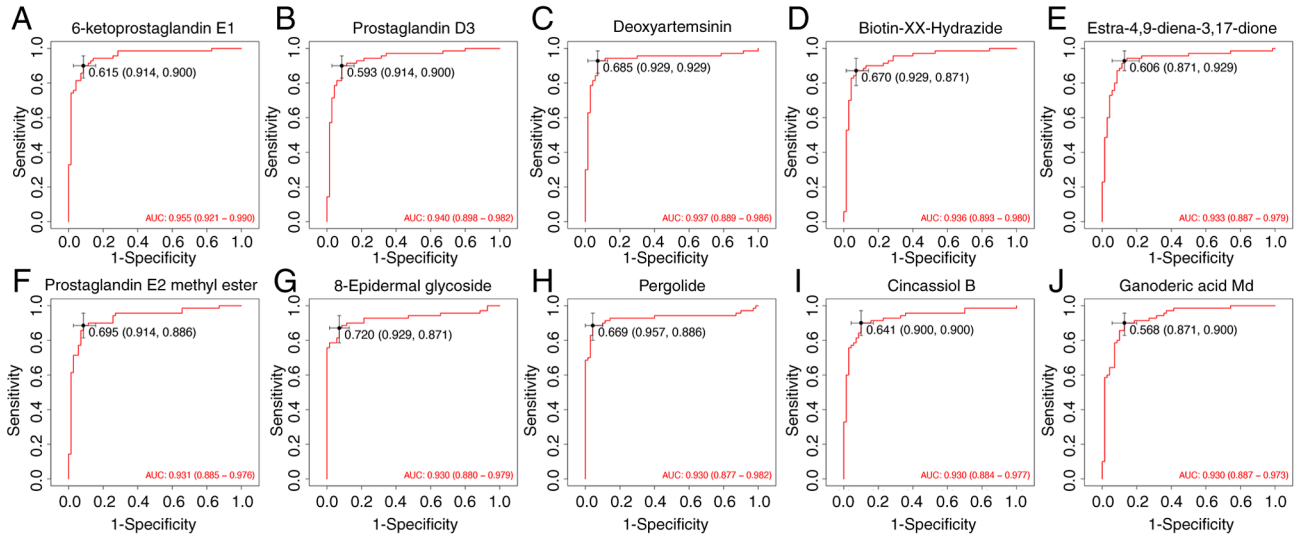

Figure 7. ROC curve analysis of 10 candidate metabolites distinguishing the NC and OB groups. ROC curves between the NC and OB groups were generated for the following metabolites: (A) 6-ketoprostaglandin E1, (B) prostaglandin D3, (C) deoxyartemisinin, (D) biotin-XX-hydrazide, (E) estra-4,9-diene-3,17-dione, (F) prostaglandin E2 methyl ester, (G) 8-epidermal glycoside, (H) pergolide, (I) cincassiol B, and (J) ganoderic acid Md. Values in black on the ROC curves indicate the optimal cut-off value, followed by the corresponding sensitivity and specificity in parentheses. ROC, receiver operating characteristic; NC, normal control; OB, refractory ascites group; AUC, area under the curve.

disruptions across both domains. This allowed for direct alignment of taxonomic and functional microbial traits with associated metabolic readouts, thereby delivering a more integrative view of gut-liver axis dysfunction. Such methodological synergy enhances the ability to identify both mechanistic drivers and therapeutic targets, paving the way for precision interventions, such as probiotic formulations, dietary modulation or microbiota transplantation, to restore microbial equilibrium and improve outcomes.

Table V. Pearson correlation analysis between refractory ascites and clinical parameters.

Parameter	Correlation coefficient (r)	P-value
PT	0.536	<0.001
INR	0.533	<0.001
TBIL	0.384	0.001
Albumin (g/l)	-0.299	0.012
Urea nitrogen	0.285	0.019
Sodium (mmol/l)	-0.27	0.024
Diagnosis	0.229	0.056
Potassium (mmol/l)	0.218	0.070
Creatinine	0.105	0.393
ALT	0.028	0.817
Age	-0.024	0.841
Sex	-0.012	0.919
AST	-0.012	0.920

PT, prothrombin time; INR, international normalized ratio; TBIL, total bilirubin; ALT, alanine aminotransferase; AST, aspartate aminotransferase.

Despite the contributions of the present study, certain limitations should be acknowledged. The cross-sectional design inherently limits causal inference. Although the cohort size exceeds that of several related studies, broader multi-center validation is necessary. Additionally, experimental validation via targeted functional assays or host-microbiome interaction models is essential to confirm mechanistic interpretations. Future efforts should also explore targeted modulation of specific microbial communities, including the role of pathogenic Enterobacteriaceae, in attenuating disease progression. Intervention-based trials with dietary fiber, microbiota-derived postbiotics or strain-level probiotics may offer feasible therapeutic routes. Future directions should also include longitudinal follow-up, interventional trials targeting microbiota or metabolism and integration with host transcriptomic and immunological profiling. Furthermore, adoption of mNGS and whole-genome metagenomics may refine taxonomic resolution and uncover rare but clinically relevant taxa. Another limitation of the present study is the absence of a direct comparison between cirrhotic patients with ascites and those with refractory ascites. Such a comparison could provide specific microbial and metabolic alterations that distinguish refractory ascites from standard ascites, particularly in terms of fecal metabolome and microbial function. Future research should include this comparative approach, which would enhance the understanding of the mechanisms behind refractory ascites and their resistance to conventional therapies. Furthermore, the biomarkers and therapeutic targets identified in the present study require further validation, and multicenter studies and randomized controlled trials are essential to confirm their clinical efficacy and applicability. Moreover, the role of dysbiosis and the increase in opportunistic pathogens in the progression of refractory ascites, spontaneous peritonitis and HRS remains insufficiently explored. Future studies should focus on elucidating the complex interactions within the gut-liver axis, which may uncover novel diagnostic and therapeutic targets.

In conclusion, through a combined analysis of gut microbiota and fecal metabolomics, the present study demonstrated that individuals with cirrhosis-related refractory ascites harbor marked disturbances in both microbial ecology and metabolic regulation. The microbial landscape was notably skewed toward Gram-negative, potentially pathogenic species, accompanied by a marked loss of protective anaerobic taxa. These compositional changes were accompanied by functional alterations in metabolic pathways implicated in oxidative stress balance, immune system dynamics and neurotransmitter signaling. Among the identified fecal metabolites, several showed strong discriminatory capacity, highlighting their value as potential biomarkers for early detection and clinical stratification. Together, these insights emphasize the pivotal role of gut-liver axis disruption in disease progression and support the development of targeted microbiota or metabolite-based interventions. Furthermore, the present study provides a foundation for future research aimed at developing diagnostic tools and therapeutic interventions, which could significantly impact clinical practice. The findings provide a solid scientific basis for advancing translational strategies aimed at restoring gut homeostasis and improving patient outcomes in end-stage liver disease.

Acknowledgements

Not applicable.

Funding

This work was supported by the 8th Talent Base of Guizhou Province-Qiannan Prefecture Talent Base for Infectious Disease Prevention and Control (grant no. RCJD2020-67), the Guangzhou Science and Technology Program (grant no. 202103000060) and the Science and Technology Fund of Guizhou Provincial Health Commission (grant no. g2wkj2023-292).

Availability of data and materials

The data generated in the present study may be found in the Genome Sequence Archive and the OMIX database of the National Genomics Data Center under accession nos. CRA029925 and OMIX011954 or at the following URLs: https://ngdc.cncb.ac.cn/gsa/browse/CRA029925 and https://ngdc.cncb.ac.cn/omix/release/OMIX011954, respectively.

Authors' contributions

DC was responsible for conceptualization, methodology and data interpretation, and was a major contributor in writing the original draft. SL performed the formal analysis, data curation and visualization and contributed to funding acquisition and manuscript reviewing and editing. KZ conducted the investigation and was responsible for resource provision and experimental validation. KP contributed to data analysis, experimental validation and manuscript review and editing.

LZ supervised the project, contributed to study design and data interpretation, and administered the overall study. DS carried out methodology development, investigation and data curation. JZ contributed to data visualization and formal analysis. DR was involved in study conceptualization, critical interpretation of data and supervised the study. DC and SL confirm the authenticity of all the raw data. All authors have read and approved the final version of the manuscript.

Ethics approval and consent to participate

Ethical approval was granted by the institutional review board of Qiannan People's Hospital (approval no. 2022-qnzy-18). Written informed consent was obtained from all human participants.

Patient consent for publication

Not applicable.

Competing interests

The authors declare that they have no competing interests.

References

1. Wong F: Management of refractory ascites. Clin Mol Hepatol 29: 16-32, 2023.
2. Zhao R, Lu J, Shi Y, Zhao H, Xu K and Sheng J: Current management of refractory ascites in patients with cirrhosis. J Int Med Res 46: 1138-1145, 2018.
3. Zaccherini G, Tufoni M, Iannone G and Caraceni P: Management of ascites in patients with cirrhosis: An update. J Clin Med 10: 5226, 2021.
4. Rajesh S, George T, Philips CA, Ahamed R, Kumbar S, Mohan N, Mohanan M and Augustine P: Transjugular intrahepatic portosystemic shunt in cirrhosis: An exhaustive critical update. World J Gastroenterol 26: 5561-5596, 2020.
5. Debernardi Venon W, Lo Pumo S, Imperatrice B, Giorgi M, Righi D, Fonio P, Saracco GM and Marzano A: Transjugular intrahepatic portosystemic shunt in refractory ascites: Clinical impact of left ventricular diastolic dysfunction. Eur J Gastroenterol Hepatol 33 (1S Suppl 1): e464-e470, 2021.
6. Gu L, Yin X, Cheng Y, Wang X, Zhang M, Zou X, Wang L, Zhuge Y and Zhang F: Overweight/Obesity increases the risk of overt hepatic encephalopathy after transjugular intrahepatic portosystemic shunt in cirrhotic patients. J Pers Med 13: 682, 2023.
7. Tranah TH, Edwards LA, Schnabl B and Shawcross DL: Targeting the gut-liver-immune axis to treat cirrhosis. Gut 70: 982-994, 2021.
8. Usuda H, Okamoto T and Wada K: Leaky gut: Effect of dietary fiber and fats on microbiome and intestinal barrier. Int J Mol Sci 22: 7613, 2021.
9. Ma L, Ni Y, Wang Z, Tu W, Ni L, Zhuge F, Zheng A, Hu L, Zhao Y, Zheng L and Fu Z: Spermidine improves gut barrier integrity and gut microbiota function in diet-induced obese mice. Gut Microbes 12: 1-19, 2020.
10. Guan H, Zhang X, Kuang M and Yu J: The gut-liver axis in immune remodeling of hepatic cirrhosis. Front Immunol 13: 946628, 2022.
11. Nishimura N, Kaji K, Kitagawa K, Sawada Y, Furukawa M, Ozutsumi T, Fujinaga Y, Tsuji Y, Takaya H, Kawaratani H, *et al*: Intestinal permeability is a mechanical rheostat in the pathogenesis of liver cirrhosis. Int J Mol Sci 22: 6921, 2021.
12. Larrue H, Vinel JP and Bureau C: Management of severe and refractory ascites. Clin Liver Dis 25: 431-440, 2021.
13. Helil AS, Haile SA, Birhanu Y, Desalegn H, Desalegn DM, Geremew RA, Gebreyohannes Z, Mohammed A, Wondimagegnehu DD, Ayana G, *et al*: Bacterial profile, drug resistance pattern, clinical and laboratory predictors of ascites infection in cirrhosis patients. BMC Infect Dis 24: 528, 2024.
14. Han S, Guiberson ER, Li Y and Sonnenburg JL: High-throughput identification of gut microbiome-dependent metabolites. Nat Protoc 19: 2180-2205, 2024.
15. Beyoğlu D, Simillion C, Storni F, De Gottardi A and Idle JR: A metabolomic analysis of cirrhotic ascites. Molecules 27: 3935, 2022.
16. Guidelines on the management of ascites and complications in cirrhosis. Zhonghua Gan Zang Bing Za Zhi 25: 664-677, 2017 (In Chinese).
17. Chen Y, Yang F, Lu H, Wang B, Chen Y, Lei D, Wang Y, Zhu B and Li L: Characterization of fecal microbial communities in patients with liver cirrhosis. Hepatology 54: 562-572, 2011.
18. Althubaiti A: Sample size determination: A practical guide for health researchers. J Gen Fam Med 24: 72-78, 2023.
19. Malik M, Hnatkova K, Batchvarov V, Gang Y, Smetana P and Camm AJ: Sample size, power calculations, and their implications for the cost of thorough studies of drug induced QT interval prolongation. Pacing Clin Electrophysiol 27: 1659-1669, 2004.
20. Biau DJ, kernéis S and Porcher R: Statistics in brief: The importance of sample size in the planning and interpretation of medical research. Clin Orthop Relat Res 466: 2282-2288, 2008.
21. Weissenborn K: Hepatic encephalopathy: Definition, clinical grading and diagnostic principles. Drugs 79 (Suppl 1): S5-S9, 2019.
22. Biggins SW, Angeli P, Garcia-Tsao G, Ginès P, Ling SC, Nadim MK, Wong F and Kim WR: Diagnosis, evaluation, and management of ascites, spontaneous bacterial peritonitis and hepatorenal syndrome: 2021 practice guidance by the American Association for the study of liver diseases. Hepatology 74: 1014-1048, 2021.
23. Delanaye P, Björk J, Courbebaisse M, Couzi L, Ebert N, Eriksen BO, Dalton RN, Dubourg L, Gaillard F, Garrouste C, *et al*: Performance of Creatinine-based equations to estimate glomerular filtration rate with a methodology adapted to the context of drug dosage adjustment. Br J Clin Pharmacol 88: 2118-2117, 2022.
24. Heidrich V, Inoue LT, Asprino PF, Bettoni F, Mariotti ACH, Bastos DA, Jardim DLF, Arap MA and Camargo AA: Choice of 16S ribosomal RNA primers impacts male urinary microbiota profiling. Front Cell Infect Microbiol 12: 862338, 2022.
25. Bharti R and Grimm DG: Current challenges and best-practice protocols for microbiome analysis. Brief Bioinform 22: 178-193, 2021.
26. Kryukov K, Imanishi T and Nakagawa S: Nanopore sequencing data analysis of 16S rRNA genes using the GenomeSync-GSTK system. Methods Mol Biol 2632: 215-226, 2023.
27. Zhang T, Li H, Ma S, Cao J, Liao H, Huang Q and Chen W: The newest Oxford Nanopore R10.4.1 full-length 16S rRNA sequencing enables the accurate resolution of species-level microbial community profiling. Appl Environ Microbiol 89: e0060523, 2023.
28. Zhang W, Fan X, Shi H, Li J, Zhang M, Zhao J and Su X: Comprehensive assessment of 16S rRNA gene amplicon sequencing for microbiome profiling across multiple habitats. Microbiol Spectr 11: e0056323, 2023.
29. Bozza S, Nunzi E, Frias-Mazuecos A, Pieraccini G, Pariano M, Renga G, Mencacci A, Talesa VN, Antognelli C, Puccetti P, *et al*: SARS-CoV-2 infection is associated with Age- and Gender-specific changes in the nasopharyngeal microbiome. Front Biosci (Landmark Ed) 29: 59, 2024.
30. Johnson JS, Spakowicz DJ, Hong BY, Petersen LM, Demkowicz P, Chen L, Leopold SR, Hanson BM, Agresta HO, Gerstein M, *et al*: Evaluation of 16S rRNA gene sequencing for species and Strain-level microbiome analysis. Nat Commun 10: 5029, 2019.
31. Sanschagrin S and Yergeau E: Next-generation sequencing of 16S ribosomal RNA gene amplicons. J Vis Exp: 51709, 2014 doi: 10.3791/51709.
32. Shi P, Liu J, Liang A, Zhu W, Fu J, Wu X, Peng Y, Yuan S and Wu X: Application of metagenomic next-generation sequencing in optimizing the diagnosis of ascitic infection in patients with liver cirrhosis. BMC Infect Dis 24: 503, 2024.
33. Shi YJ, Sheng KW, Zhao HN, Liu C and Wang H: Toll-like receptor 2 deficiency exacerbates dextran sodium sulfate-induced intestinal injury through Marinifilaceae-dependent attenuation of cell cycle signaling. Front Biosci (Landmark Ed) 29): 338, 2024.

34. Gitto S, Vizzutti F, Baldi S, Campani C, Navari N, Falcini M, Venturi G, Montanari S, Roccarina D, Arena U, *et al*: Transjugular intrahepatic Porto-systemic shunt positively influences the composition and metabolic functions of the gut microbiota in cirrhotic patients. Dig Liver Dis 55: 622-628, 2023.
35. Beyoğlu D, Popov YV and Idle JR: The metabolomic footprint of liver fibrosis. Cells 13: 1333: 2024.
36. Singh R, Zogg H, Wei L, Bartlett A, Ghoshal UC, Rajender S and Ro S: Gut microbial dysbiosis in the pathogenesis of gastrointestinal dysmotility and metabolic disorders. J Neurogastroenterol Motil 27: 19-34, 2021.
37. Seo SK and Kwon B: Immune regulation through tryptophan metabolism. Exp Mol Med 55: 1371-1379, 2023.
38. Ye J, Bi X, Deng S, Wang X, Liu Z, Suo Q, Wu J, Chen H, Wang Y, Qian K, *et al*: Hypoxanthine is a metabolic biomarker for inducing GSDME-dependent pyroptosis of endothelial cells during ischemic stroke. Theranostics 14: 6071-687, 2024.
39. Roehlen N, Crouchet E and Baumert TF: Liver fibrosis: Mechanistic concepts and therapeutic perspectives. Cells 9: 875, 2020.
40. Sak JJ, Prystupa A, Bis-Wencel H, Kiciński P, Luchowska-Kocot D, Krukowski H, Nowicki GJ and Panasiuk L: Oxidative stress-induced growth inhibitor 1 in alcohol-induced liver cirrhosis. Ann Agric Environ Med 28: 676-680, 2021.
41. Blachier F: Metabolism of dietary substrates by intestinal bacteria and consequences for the host intestine. In: Metabolism of alimentary compounds by the intestinal microbiota and health. Springer, pp45-144, 2023.
42. Alonso-Peña M, Espinosa-Escudero R, Herraez E, Briz O, Cagigal ML, Gonzalez-Santiago JM, Ortega-Alonso A, Fernandez-Rodriguez C, Bujanda L, Calvo Sanchez M, *et al*: Beneficial effect of ursodeoxycholic acid in patients with acyl-CoA oxidase 2 (ACOX2) deficiency-associated hypertransaminasemia. Hepatology 76: 1259-1274, 2022.
43. Guan Z, Li Y, Hu S, Mo C, He D, Huang Z and Liao M: Screening and identification of differential metabolites in serum and urine of bamaxiang pigs bitten by trimeresurus stejnegeri based on UPLC-Q-TOF/MS metabolomics technology. J Toxicol Sci 47: 389-407, 2022.